UWB-Foot-SLAM: Bounding Position Error of Foot-mounted Pedestrian INS with Simultaneously Localized UWB Beacons

Chi-Shih Jao[1], Danmeng Wang[1], Joe Grasso[2], and Andrei M. Shkel[1]
[1]*Microsystems Lab, Department of Mechanical and Aerospace Engineering, University of California, Irvine*
Irvine, CA, USA
{chshihj,danmenw,andrei.shkel}@uci.edu
[2]*Public Safety Communications Research Division, National Institute of Standard and Technology*
Boulder, CO, USA
joseph.grasso@nist.gov

***Abstract*—This paper proposes a Simultaneous Localization And Mapping (SLAM) approach, utilizing a combination of foot-mounted Inertial Measurement Units (IMU), foot-mounted Ultra-WideBand (UWB), and environment-deployed UWBs, referred to as the UWB-Foot-SLAM. The proposed approach first leverages a Zero-velocity-UPdaTe (ZUPT)-aided Inertial Navigation System (INS) to map unknown UWB beacons deployed in an environment during navigation and then utilizes the localized beacons to bound position error propagation. An experimental testbed was developed, and we conducted two experiments to validate the performance of the proposed UWB-Foot-SLAM. Experimental results in the first experiment, which involved a pedestrian walking for 3 minutes and deploying two beacons, showed that the UWB beacons' positions estimated by the proposed UWB-Foot-SLAM had displacement errors of 0.28 [m] and 0.22 [m]. In the second experiment, a pedestrian traveled for 25 minutes in a large multi-floor indoor environment and deployed four beacons. The positions of the pedestrian estimated by ZUPT-aided INS had horizontal and vertical Loop-Closure Errors (LCEs) of 11 [m] and 4.5 [m], respectively. When our proposed UWB-Foot-SLAM was used, the LCEs were reduced to 1.49 [m] and 1 [m], respectively, and the covariances associated with the pedestrian position states were bounded after operating for 155 [s].**

***Index Terms*—IMU, UWB, SLAM, Indoor navigation, Inertial navigation**

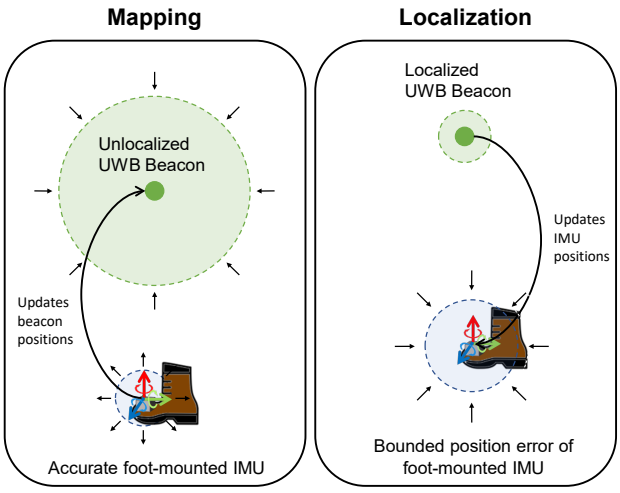

Fig. 1. Concept of the proposed UWB-Foot-SLAM.

I. Introduction

Developing an accurate and reliable universal pedestrian navigation framework can enable multiple different Location-Based Services (LBS), including contact tracing [1], warehouse inventory management [2], shopping [3], gaming [4], and firefighter tracking [5]. The universal navigation framework needs to maintain small positioning errors for a long period of time and covers various challenging scenarios, such as indoor environments, urban canyons, forest canopies, and underground caves. These scenarios often come with disadvantages in that signals of Global Navigation Satellite Systems (GNSS) are degraded or unavailable, visibility is poor due to smoke or low light intensity, and infrastructures dedicated to navigation are not accessible. These conditions constrain the usability of many existing positioning technologies, including cameras [6], Light Detection and Ranging (LiDAR) [7], Radio-Frequency (RF) systems based on Bluetooth [8], Wi-Fi [9], cellular Long-Term Evolution (LTE) [10], or Ultra-WideBand (UWB) [11], and Inertial Navigation Systems (INS) [12]. In order to operate through extreme conditions, integrating positioning technologies that have complementary localization properties is considered as a potential solution [13].

INS is a popular option to be integrated into such a navigation system as it operates in a self-contained manner, requires no installation time, and provides consistently available measurements. Nevertheless, errors of a standalone INS accumulate over time, causing the navigation solution to eventually drift unboundedly [14]. In pedestrian navigation, an aiding technique that reduces the rate of error growth of an INS is a Zero-velocity-UPdaTe (ZUPT) algorithm [15], which uses foot-mounted Inertial Measurement Units (IMUs) and periodically resets velocity errors during the stance phases of a human gait cycle [16]. The ZUPT-aided INS has been analytically predicted and experimentally demonstrated to achieve an error

of less than 1% of the traveling distance with an industrial-grade IMU [17]. However, the ZUPT-aided INS was proven to have unbounded position and yaw angle error growths [18]. The positioning solutions of a standalone ZUPT-aided INS eventually drift, and additional enhancement techniques are needed for long-term navigation tasks.

In order to bound position error growths of ZUPT-aided INS, various sensor fusion solutions that opportunistically utilize exteroceptive external RF signals were developed [19]. Among a variety of RF signals, UWB is often considered a preferable aiding source for its properties of high bandwidth, low time resolutions, and the capability to operate under both Line-of-Sight (LoS) Non-LoS (NLoS) conditions [20]. Previous research work has shown that integrating UWB and foot-mounted INS could be mutually beneficial [21]. On the one hand, the navigation solutions of ZUPT-aided INS using foot-mounted IMUs could be used to enhance the reliability of UWB-based localization systems under NLoS scenarios [22]. On the other hand, fusing UWB range measurements transmitted from pre-deployed beacons with foot-mounted IMUs could globally bound position error growth [23], extending positioning accuracy in long-term navigation. Many integration schemes were developed, including loosely- or tightly-coupled frameworks implemented with different estimation filters, such as Extended Kalman Filter (EKF) [21], [24]–[26], Particle Filter [27], and Graph Optimization [23]. While these solutions effectively constrain position errors of the ZUPT-aided INS, the proposed approaches assumed that UWB beacons were pre-installed in the navigation environment and the locations of the beacons were pre-surveyed. Surveying locations of beacons usually requires expensive external positioning devices, such as motion cameras or LiDAR, and the process is time-consuming. Therefore, it is not always possible to be performed in emergency situations. Localization systems integrating UWB and foot-mounted IMUs in their current forms are not a preferable candidate as a universal navigation framework.

This paper proposes an algorithm of Simultaneous Localization And Mapping using both UWBs and foot-mounted IMUs referred to as UWB-Foot-SLAM. The proposed UWB-Foot-SLAM, illustrated in Fig. 1, is designed to use UWB range measurements to bound position errors of ZUPT-aided INS using foot-mounted IMUs without the need to pre-deploy and pre-survey the UWB beacons. The proposed UWB-Foot-SLAM algorithm considers that a pedestrian performing navigation is equipped with hardware consisting of a foot-mounted platform that integrates an IMU and a UWB module and multiple standalone UWB beacons. During a navigation task, the pedestrians deploy the unknown UWB beacons in the environments. The proposed UWB-Foot-SLAM algorithm sets locations of these UWB beacons as states to be estimated in an EKF framework and leverages a property of the ZUPT-aided INS that the system has very high position accuracy at the beginning of an operation. During this period, the localization solution of the ZUPT-aided INS is used to estimate unknown UWB beacons' locations based on range measurements between the foot-mounted UWB and the UWB beacons. When the estimation uncertainty of the UWB beacon's location reaches a sufficiently low value, the UWB range measurements are used to provide position compensation for the ZUPT-aided INS. This paper has the following contributions:

- Developing an EKF framework that simultaneously localizes unknown UWB beacons using ZUPT-aided INS
- Developing a hardware system that realizes implementation of the proposed UWB-Foot-SLAM algorithm, and
- Performing real-world indoor pedestrian navigation experiments to validate navigation performance of the proposed algorithm.

This paper is organized as follows. Section II describes the algorithm of the proposed UWB-Foot-SLAM, Section III discusses a hardware prototype developed to validate the proposed algorithm, Section IV presents the results of two different experiments, and Section V concludes the paper with a highlight of the results.

II. Algorithm Design

A. Overview

The proposed UWB-Foot-SLAM simultaneously localizes a pedestrian's positions and maps positions of unknown beacons with measurements collected from a foot-mounted IMU, a foot-mounted UWB sensor, and several UWB sensors to be deployed in a surrounding environment during navigation. Fig. 2 shows a block diagram illustrating the proposed UWB-Foot-SLAM algorithm. To differentiate UWB sensors for different usages, we will refer to a UWB sensor mounted on the foot as a foot-mounted UWB and a UWB deployed in a navigation environment as a UWB beacon in the rest of the text. We consider a UWB beacon to have two statuses: *unlocalized* and *localized*. An unlocalized UWB beacon has an estimated position uncertainty significantly larger than the position uncertainty of a foot-mounted IMU, while the position uncertainty of a localized UWB beacon is similar to or smaller than that of the foot-mounted IMU. All of the UWB beacons when first deployed are considered to be in the unlocalized status.

In our proposed UWB-Foot-SLAM, localization of a pedestrian utilizes a combination of the ZUPT-aided INS and foot-to-beacon range measurements collected from a pair of foot-mounted UWB and a localized UWB beacon. If a UWB beacon is in the unlocalized status, its range measurements would have minimal numerical impacts on the estimated pedestrian's positions. Mapping of the proposed UWB-Foot-SLAM estimates unlocalized beacons' positions using the knowledge of a pedestrian's current position and foot-to-beacon range measurements collected from a pair of foot-mounted UWB and the unlocalized UWB beacons. The localization and mapping steps are both achieved with an EKF. After initialization of the EKF, the filter enters the mapping step. In this step, the uncertainties of the UWB position states are reduced, and the uncertainties of the foot-mounted IMU position states increase. After operating for a while, the filter performs the localization

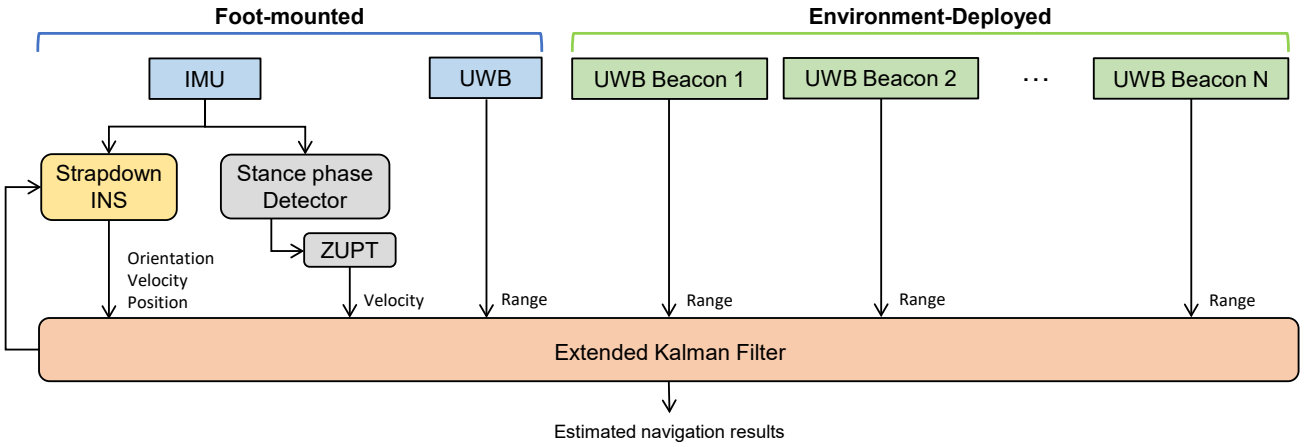

Fig. 2. Block diagram illustrating the proposed UWB-Foot-SLAM algorithm. The algorithm involved a foot-mounted IMU, a foot-mounted UWB, and several UWB beacons to be deployed in an operating environment during a navigation task.

step, and the position error growth of the foot-mounted IMU is bounded.

B. Extended Kalman Filter

The proposed UWB-Foot-SLAM algorithm is realized in an EKF framework, shown in Fig. 2. N number of beacons are assumed to be involved in a navigation task.

1) Filter states: The EKF uses states that includes orientations, velocities, and positions of a foot-mounted IMU as well as the positions of UWB beacons. The states are expressed as follows:

$$\mathbf{x}_k = \begin{bmatrix} \mathbf{q}_k^\top & \mathbf{v}_k^\top & \mathbf{p}_k^\top & \mathbf{b}_{\mathrm{g},k}^\top & \mathbf{b}_{\mathrm{a},k}^\top & \mathbf{p}_{\mathrm{B}_1,k}^\top & \cdots & \mathbf{p}_{\mathrm{B}_N,k}^\top \end{bmatrix}^\top,$$

where $\mathbf{q}_k$, $\mathbf{v}_k$, and $\mathbf{p}_k \in \mathbb{R}^{3\times1}$ are the orientation, velocity, and position states of an agent expressed in the navigation frame. $\mathbf{b}_{\mathrm{g},k}$ and $\mathbf{b}_{\mathrm{a},k} \in \mathbb{R}^{3\times1}$ are the gyroscope and accelerometer biases along the three axes of the IMU body frame. $\mathbf{p}_{\mathrm{B}_1,k}, \ldots, \mathbf{p}_{\mathrm{B}_N,k} \in \mathbb{R}^{3\times1}$ represent the position of the N UWB beacons being deployed.

2) Filter Initialization: In the beginning of a navigation task, we assumed a pedestrian would remain stationary for a short period. The initial roll angle, θ_0, and pitch angle, ϕ_0, are expressed as follows:

$$\theta_0 = \tan^{-1}\left(\frac{-\bar{\mathbf{a}}_y}{-\bar{\mathbf{a}}_z}\right), \phi_0 = \tan^{-1}\left(\frac{\bar{\mathbf{a}}_x}{\sqrt{\bar{\mathbf{a}}_y^2 + \bar{\mathbf{a}}_z^2}}\right),$$

where $\bar{\mathbf{a}}_i$ indicate the averaged ith-axis accelerometer readings collected during the initialization period. The initial yaw angle, ψ_0, can be determined with additional sensors, such as a magnetometer. The initial position, $\mathbf{p}_0$, and velocity, $\mathbf{v}_0$, can be determined with external localization systems. Accelerometer states, $\mathbf{b}_{\mathrm{a},0}$, is set to zeros. Initial gyroscope biases, $\mathbf{b}_{\mathrm{g},0}$, are expressed as

$$\mathbf{b}_{\mathrm{g},0} = \begin{bmatrix} \bar{\boldsymbol{\omega}}_x & \bar{\boldsymbol{\omega}}_y & \bar{\boldsymbol{\omega}}_z \end{bmatrix}^\top,$$

where $\bar{\boldsymbol{\omega}}_i$ indicates the averaged ith-axis gyroscope readings collected during the initialization period.

When a UWB beacon with an identification (ID) number j is first connected to the foot-mounted UWB at time k, the proposed UWB-Foot-SLAM sets the initial beacon positions, denoted as $\mathbf{p}_{\mathrm{B}_j,0}$, with the current position of the foot-mounted IMU, $\mathbf{p}_k$. The corresponding initial position uncertainties, $\sigma_{\mathbf{p}_{\mathrm{B}_j},0}$, are initialized with the size of a navigation environment. $\mathbf{p}_{\mathrm{B}_j,0}$ and $\sigma_{\mathbf{p}_{\mathrm{B}_j},0}$ are expressed as follows.

$$\mathbf{p}_{\mathrm{B}_j,0} = \mathbf{p}_k, \sigma_{\mathbf{p}_{\mathrm{B}_j},0} = \mathrm{A},$$

where A is the dimension of a navigation environment.

3) Prediction Step: In the prediction step of the EKF, the states corresponding to the foot-mounted IMU, including $\mathbf{q}_k, \mathbf{v}_k, \mathbf{p}_k, \mathbf{b}_{\mathrm{g},k}$, and $\mathbf{b}_{\mathrm{a},k}$, are propagated with the strapdown INS algorithm [12]. The position states of the beacons are assumed constant. The EKF propagation matrix, denoted by $\mathbf{A}_k$, is expressed as follows

$$\mathbf{A}_k = \begin{bmatrix} \mathbf{A}_{\mathrm{INS},k} & \mathbf{0}_{15\times3N} \\ \mathbf{0}_{3N\times15} & \mathbf{0}_{3N\times3N} \end{bmatrix}$$

$$\mathbf{A}_{\mathrm{INS},k} = \begin{bmatrix} \mathbf{0}_{3\times3} & \mathbf{0}_{3\times3} & \mathbf{0}_{3\times3} & -\mathrm{C}(\mathbf{q}_k) & \mathbf{0}_{3\times3} \\ [\overrightarrow{f}^n\times] & \mathbf{0}_{3\times3} & \mathbf{0}_{3\times3} & \mathbf{0}_{3\times3} & \mathrm{C}(\mathbf{q}_k) \\ \mathbf{0}_{3\times3} & \mathbf{I}_{3\times3} & \mathbf{0}_{3\times3} & \mathbf{0}_{3\times3} & \mathbf{0}_{3\times3} \\ \mathbf{0}_{3\times3} & \mathbf{0}_{3\times3} & \mathbf{0}_{3\times3} & \mathbf{0}_{3\times3} & \mathbf{0}_{3\times3} \\ \mathbf{0}_{3\times3} & \mathbf{0}_{3\times3} & \mathbf{0}_{3\times3} & \mathbf{0}_{3\times3} & \mathbf{0}_{3\times3} \end{bmatrix}.$$

Here, $[\overrightarrow{f}^n\times]$ is the skew-symmetric cross-product-operator of the accelerometer outputs of the IMU, expressed in the navigation frame. $\mathrm{C}(\mathbf{q})$ is the Directional Cosine Matrix (DCM) corresponding to the quaternion vector $\mathbf{q}$. $\mathbf{0}_{n\times m}$ indicates a zero matrix having n number of rows and m number of columns. The corresponding process noise matrix, denoted as $\mathbf{Q}_k$, is expressed as

$$\mathbf{Q}_k = \begin{bmatrix} \mathbf{Q}_{\mathrm{INS},k} & \mathbf{0}_{15\times3N} \\ \mathbf{0}_{3N\times15} & \mathbf{0}_{3N\times3N} \end{bmatrix},$$

with $\mathbf{Q}_{\text{INS},k} =$

$$\begin{bmatrix} \sigma^2_{\text{ARW}}\mathbf{I}_{3\times3} & \mathbf{0}_{3\times3} & \mathbf{0}_{3\times3} & \mathbf{0}_{3\times3} & \mathbf{0}_{3\times3} \\ \mathbf{0}_{3\times3} & \sigma^2_{\text{VRW}}\mathbf{I}_{3\times3} & \mathbf{0}_{3\times3} & \mathbf{0}_{3\times3} & \mathbf{0}_{3\times3} \\ \mathbf{0}_{3\times3} & \mathbf{I}_{3\times3} & \mathbf{0}_{3\times3} & \mathbf{0}_{3\times3} & \mathbf{0}_{3\times3} \\ \mathbf{0}_{3\times3} & \mathbf{0}_{3\times3} & \mathbf{0}_{3\times3} & \sigma^2_{\text{AcRW}}\mathbf{I}_{3\times3} & \mathbf{0}_{3\times3} \\ \mathbf{0}_{3\times3} & \mathbf{0}_{3\times3} & \mathbf{0}_{3\times3} & \mathbf{0}_{3\times3} & \sigma^2_{\text{RRW}}\mathbf{I}_{3\times3} \end{bmatrix}.$$

Here, $\mathbf{I}_{n\times n}$ is the identity matrix having n number of rows and columns. σ^2_{ARW}, σ^2_{VRW}, σ^2_{RRW}, and σ^2_{AcRW} are the Angle Random Walk (ARW) of the gyroscopes, the Velocity Random Walk (VRW) of the accelerometers, the Rate Random Walk (RRW) of the gyroscopes, and the Acceleration Random Walk (AcRW) of the accelerometers of the foot-mounted IMU.

4) Update Step: When a stance phase is detected, the ZUPT algorithm is activated to compensate for the velocity state in the update step of the EKF. The compensation is done by feeding in pseudo-measurements of zero velocity along the three axes, which is denoted as $\mathbf{v}_{\text{ZUPT},k} = \mathbf{0}_{3\times1}$. In this paper, the stance phase detection is achieved with the Stance Hypothesis Optimal dEtection (SHOE) detector [28], which determines a stance phase if a test statistics, $T(\mathbf{u}_n) =$

$$\frac{1}{M}\sum_{k\in\Omega_n}\left(\frac{1}{\sigma^2_{\text{VRW}}}\parallel \mathbf{y}^\alpha_k - g\frac{\bar{\mathbf{y}}^\alpha_k}{\parallel \bar{\mathbf{y}}^\alpha_k \parallel}\parallel^2 + \frac{1}{\sigma^2_{\text{ARW}}}\parallel \mathbf{y}^\omega_k \parallel^2\right) < \gamma,$$

where $\mathbf{u}_n = \{\mathbf{y}_k\}_{k=n}^{k=N-1}$ with $\mathbf{y}_k = [\mathbf{y}^\alpha_k, \mathbf{y}^\omega_k]^\top$, $\mathbf{y}^\alpha_k$ is 3-axis accelerometer measurements at time k, $\mathbf{y}^\omega_k$ is 3-axis gyroscope measurements at time k, g is the gravitational constant, $\Omega_n = \{l \in \mathbb{N}, n \le l < M-1\}$ is a collection of the sensor measurement indexes at time n with a window of length M, and γ are user-defined thresholds.

The ZUPT measurement models, $\mathbf{z}_{\text{ZUPT},k}$, measurement matrices, $\mathbf{H}_{\text{ZUPT},k}$, and measurement covariance matrices, $\mathbf{R}_{\text{ZUPT},k}$ are expressed as follows:

$$\mathbf{z}_{\text{ZUPT},k} = \mathbf{v}_{\text{ZUPT},k}$$

$$\mathbf{H}_{\text{ZUPT},k} = \begin{bmatrix}\mathbf{0}_{3\times3} & \mathbf{I}_{3\times3} & \mathbf{0}_{(9+3N)\times3}\end{bmatrix}$$

$$\mathbf{R}_{\text{ZUPT},k} = \sigma^2_{\text{ZUPT}}\mathbf{I}_{3\times3},$$

where σ^2_{ZUPT} is the noise variance of the zero-velocity measurement $\mathbf{v}_{\text{ZUPT}}$.

When a ith UWB measurement, denoted as $r_{\text{UWB}_i,k}$, becomes available, the measurements are first classified into LoS and NLoS cases, and only LoS cases are used in the update step of the EKF. This paper uses a probabilistic power metric approach to differentiate LoS and NLoS UWB measurements [29]. The LoS measurements are further processed with bias correction through a curve-fitting approach. The corresponding foot-to-beacon range measurement model, $z_{\text{UWB}_i,k}$, measurement matrix, $\mathbf{H}_{\text{UWB}_i,k}$, and measurement noise matrix, $\mathbf{R}_{\text{UWB}_i,k}$, are described as follows:

$$z_{\text{UWB}_i,k} = r_{\text{UWB}_i,k}$$

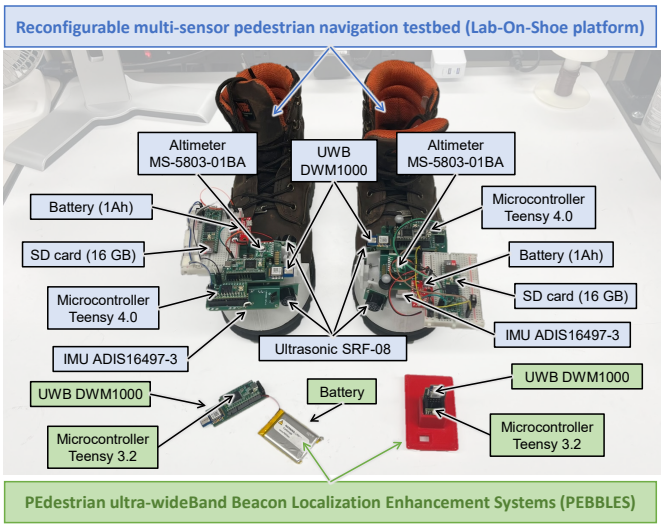

Fig. 3. Experimental setup. The setup included the Lab-On-Shoe platform and the PEBBLE system. The Lab-On-Shoe platform included multiple sensing modalities. This paper only used the IMU and UWB mounted on the left foot.

$$\mathbf{H}_{\text{UWB}_i,k} = \begin{bmatrix} \mathbf{0}_{6\times1} \\ \frac{\partial||\mathbf{p}_k - \mathbf{p}_{\text{B}_i,k}||^\top}{\partial \mathbf{p}_k} \\ \mathbf{0}_{(6+3(i-1))\times1} \\ \frac{\partial||\mathbf{p}_k - \mathbf{p}_{\text{B}_i,k}||^\top}{\partial \mathbf{p}_{\text{B}_i,k}} \\ \mathbf{0}_{3(N-i-1)\times1} \end{bmatrix}^\top$$

$$\mathbf{R}_{\text{UWB}_i,k} = \sigma^2_{\text{UWB}_i},$$

where $\sigma^2_{\text{UWB}_i}$ is the noise variance of the foot-to-beacon range measurements between the foot-mounted UWB and the ith UWB beacon.

III. System Design

To realize the proposed UWB-Foot-SLAM algorithm, we developed a reconfigurable multi-sensor pedestrian navigation testbed, referred to as the Lab-On-Shoe platform, and multiple integrated UWB beacon units, referred to as PEdestrian ultra-wideBand Beacon Localization Enhancement (PEBBLE) systems. This section discusses both the hardware and firmware implementation of the developed prototype.

A. Hardware Implementation

Fig. 3 presents the developed experimental prototypes. The Lab-On-Shoe platform was previously developed as a flexible hardware testbed at the Microsystem Laboratory at the University of California, Irvine, with the purpose of investigating sensor fusion solutions for integrated pedestrian inertial navigation system [13], [19], [30]. In this paper, we upgraded the platform. On each shoe, we integrated multiple Commercial-Off-The-Shelf (COTS) components, including three Teensy micro-controllers, an Analog Device IMUs ADIS16497-3, a barometric altimeter MS-5803-01BA, two ultrasonic range sensor SRF02, a UWB module DWM1000, and a Secure Digital (SD) card. The three Teensy microcontrollers are Teensy

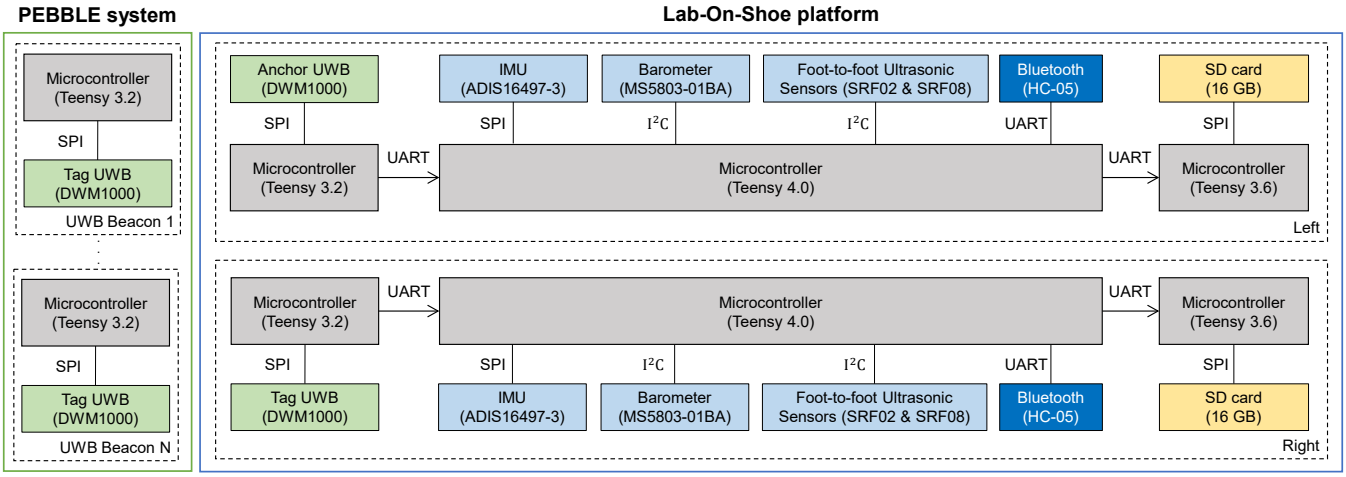

Fig. 4. Block diagram illustrating firmware of the Lab-On-Shoe platform and the PEBBLE system.

4.0, Teensy 3.6, and Teensy 3.2, having Central Processing Unit (CPU) clock rates of 600 [MHz], 180 [MHz], and 96 [MHz], respectively. The SD card module was a built-in module on the Teensy 3.6 microcontroller. All the components were firmly mounted on a customized 3D-printed PolyLactic Acid (PLA) fixture. Each UWB beacon in the PEBBLE system included a microcontroller Teensy 3.2 and a UWB module DWM1000. The Lab-On-Shoe platform and the PEBBLE system were both powered up with 5.0-V lithium-ion batteries.

B. Firmware Implementation

Fig. 4 presents a block diagram describing firmware schematics implemented on the Lab-On-Shoe platform and the PEBBLE system. On the Lab-On-Shoe platform, the Teensy 3.2 microcontroller collected information on the connected node ID number and measurements of range, transmitter power, receiver first pulse power, and power metrics at a rate of 10 [Hz] from the DWM1000 UWB module via the Serial Peripheral Interface (SPI) communication protocol. The DWM1000 module mounted on the left shoe was programmed to operate in the anchor mode, and the module mounted on the right shoe was in the tag mode. The collected measurements were transmitted to the Teensy 4.0 microcontroller via the Universal Asynchronous Receiver-Transmitter (UART) communication protocol. On the Teensy 4.0 microcontroller, we implemented the SPI protocol to collect IMU measurements at a rate of 1000 [Hz] as well as the Inter-Integrated Circuit (I^2C) communication protocol to collect pressure and thermal measurements from the MS5803-01BA barometer at a rate of 25 [Hz] and inter-foot ranging measurements from the two SRF02 ultrasonic sensors at a rate of 25 [Hz]. After all the sensor measurements were collected at each implementation loop, the Teensy 4.0 transmitted the measurements to the Teensy 3.6 microcontroller via UART communication protocol. The Teensy 3.6 microcontroller implemented the SPI protocol to write all the received measurements to an SD card.

On the PEBBLE system, the Teeny 3.2 microcontroller implemented the SPI communication protocol to collect information on the connected node ID number and measurements of range, transmitter power, receiver first pulse power, and power metrics at a rate of 10 [Hz]. All the UWB modules in the developed PEBBLE system were programmed to operate in the tag mode. A DWM1000 UWB operating in the tag mode can only be paired with a UWB operated in the anchor mode, and the range measurements between the two UWBs were obtained through a two-way ranging method. Therefore, all the UWB modules involved in the PEBBLE system, when within a detectable range, were connected only to the UWB mounted on the left shoe of the Lab-On-Shoe platform.

IV. Experimental Validation

We conducted two experiments to validate the proposed UWB-Foot-SLAM using the developed Lab-On-Shoe platform and the PEBBLE system.

A. Scenarios #1: A small area with reference motion capture cameras

In the first experiment, a subject was equipped with the Lab-On-Shoe platform and carried two UWB beacons. Fig. 5 shows the experimental scenario. The subject walked a close-loop trajectory along a square shape in a 6 [m] by 6 [m] area for around 3 minutes, resulting in a trajectory length of around 140 [m]. In the beginning of the experiment, the subject stood still at the origin for 10 seconds. Two beacons, denoted as beacon #1 and beacon #2, were deployed at the beginning of the experiment. The first LoS range measurements of beacon #1 were collected at the 15 [s] timestamp, and the LoS measurements of beacon #2 were collected at the 20 [s] timestamp. A set of OptiTrack motion capture cameras was used to obtain the ground truth positions of the two beacons and the subject's feet. The sampling rate of the camera system was 120 [Hz]. In this experiment, among all the measurements produced by the Lab-On-Shoe platform, we only used the ones collected by the IMU and UWB mounted on the left shoe.

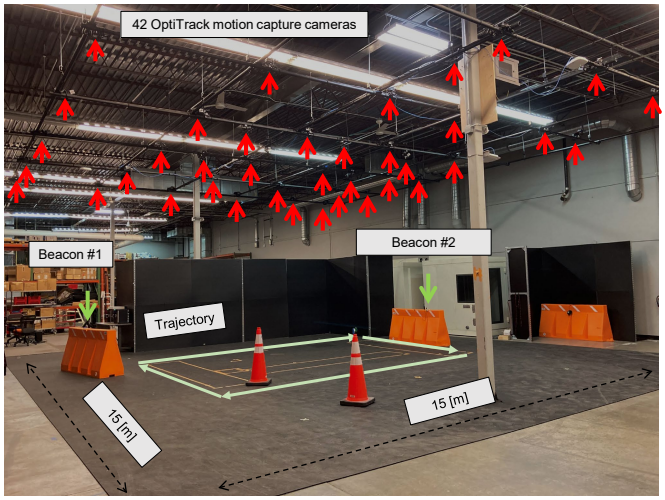

Fig. 5. Experimental scenario for the experiment discussed in Section IV-A. 42 OptiTrack motion capture cameras were mounted on the ceiling of a warehouse and obtain the ground truth position and orientation. Two beacons were placed on top of the orange barricades during the experiment. A pedestrian performed the experiment by walking along the light green trajectory.

We compared the navigation solutions computed by our proposed UWB-Foot-SLAM algorithm with a standalone ZUPT-aided INS. The initial yaw angle and positions used in the estimated solutions were aligned with the coordinate system of the motion capture cameras. The EKF parameters used in this paper are summarized in TABLE I. Fig. 6 presents the two navigation solutions. The ZUPT-aided INS solution only estimated the positions of the agent while the proposed UWB-Foot-SLAM estimated both the agent's and beacons' positions. We used ground truth positions provided by the motion capture cameras to evaluate the accuracy of the estimated navigation solutions. Agent's positions estimated by the ZUPT-aided INS had a 2D Root-Mean-Squared-Error (RMSE) of 0.15 [m], a 2D final displacement error of 0.22 [m], and a 2D maximum displacement error of 0.37 [m]. The positions estimated by the proposed UWB-Foot-SLAM had a 2D RMSE, 2D final displacement error, and a 2D maximum displacement error of 0.15 [m], 0.27 [m], and 0.31 [m], respectively. Beacons' positions estimated by the proposed UWB-Foot-SLAM had 2D final displacement errors of 0.28 [m] for beacon #1 and 0.22 [m] for beacon #2.

TABLE I
PARAMETERS FOR THE EKF

Hyper-parameter	Value
σ_{ARW}	2.7221×10^{-5}
σ_{VRW}	0.0017
σ_{RRW}	8.3174×10^{-7}
σ_{AcRW}	6.63×10^{-6}
σ_{ZUPT}	0.02
σ_{UWB_i}	0.5

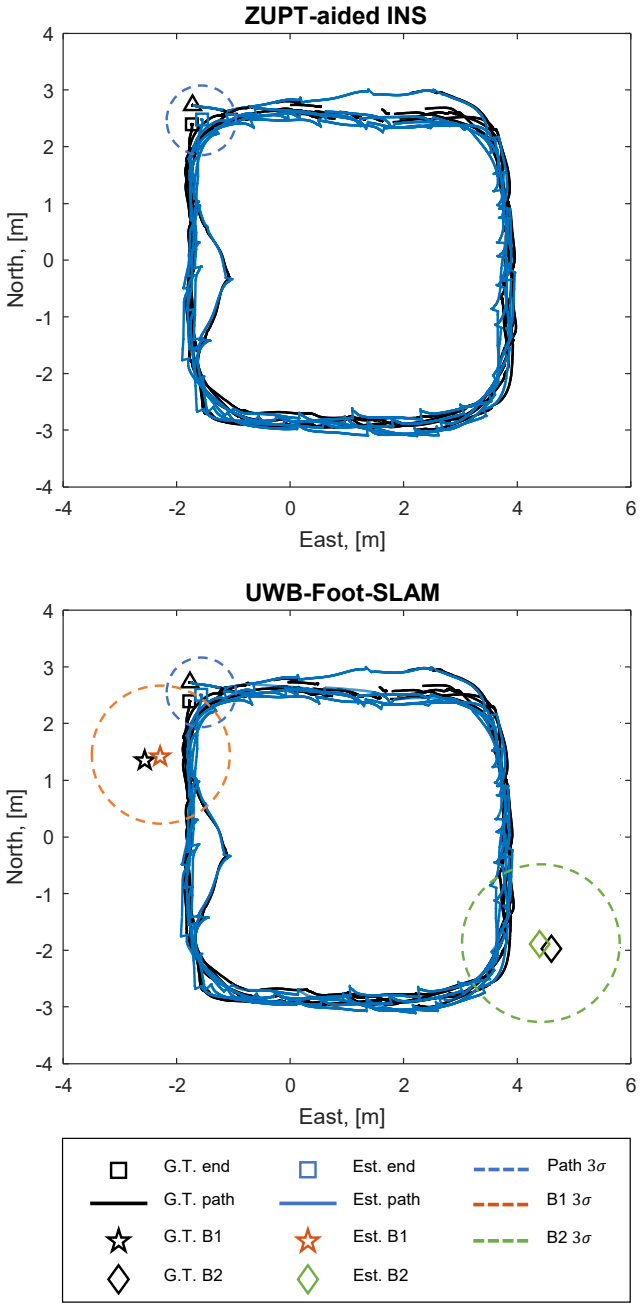

Fig. 6. Estimated (Est.) Navigation solutions computed with a standalone ZUPT-aided INS and the proposed UWB-Foot-SLAM in the experiment discussed in Section IV-A. Items colored in black correspond to the Ground Truth (G.T.) collected by motion capture cameras. The radius of each dashed circle represents three times the position standard deviation. Positions of Beacon #1 (B1) and beacon #2 (B2) are marked with star and diamond symbols, respectively.

Fig. 7 presents the covariances associated with the position states of the agent and the beacons when using the proposed UWB-Foot-SLAM algorithm. We could see that the uncertainties of the agent's positions grew over time while the beacons' position uncertainties decreased. In this experiment, the proposed UWB-Foot-SLAM was considered to operate

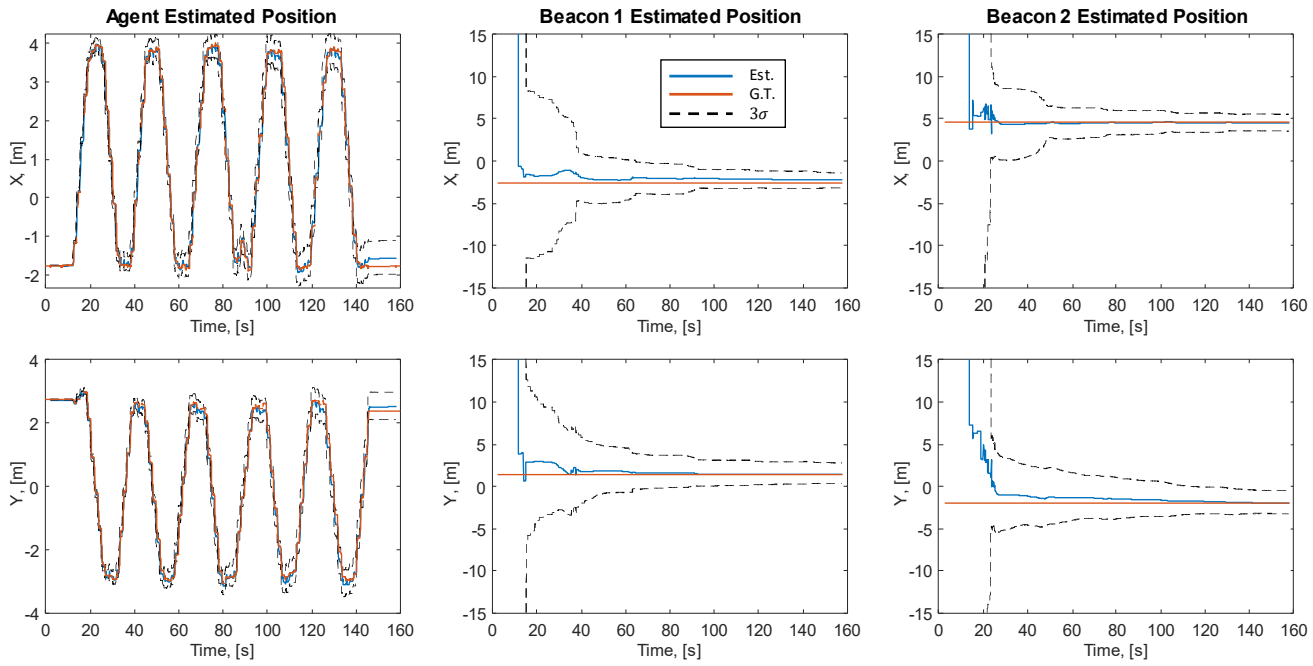

Fig. 7. Position estimates and its associated covariances of the proposed UWB-Foot-SLAM algorithm in the experiment discussed in Section IV-A. It could be observed that the covariances of the agent's positions increased over time while the covariances of the beacons' positions were reduced. At the end of this experiment, the covariances of the agent's positions were still less than that of the beacons' locations.

in the mapping mode, as the agent's position uncertainties had not grown beyond the beacons' position uncertainties at the end of the experiment. Therefore, the UWB range measurements did not have significant numerical impacts on the agent's estimated positions.

B. Scenarios #2: A large area including multiple floors

In the second experiment, the subject walked a closed-loop trajectory in a building on two different floors covering terrains of flat planes, stairs, and ramps. The experimental scenario had a physical dimension of approximately 70 [m] by 25 [m] by 6 [m]. The duration was around 25 minutes, and the trajectory length was approximately 1.5 [km]. The subject started the experiment on the second floor of the building and distributed four UWB beacons at different locations on the first and second floors of the building. Beacon #1, #2, #3, and #4 were deployed at timestamps of 21 [s], 72 [s], 197 [s], and 266 [s]. Beacon #1 and #2 were deployed on the first floor, and beacon #3 and #4 two were deployed on the second floor.

Fig. 8 shows the navigation solutions estimated by the standalone ZUPT-aided INS and the proposed UWB-Foot-SLAM. The 2D Loop-Closure Error (LCE) of the agent's positions was 11 [m] when estimated by the ZUPT-aided INS and 1.49 [m] when estimated by our proposed UWB-Foot-SLAM algorithm. The vertical displacement error was 4.5 [m] in the case of the ZUPT-aided INS and 1.09 [m] in the case of the UWB-Foot-SLAM. The positions of the deployed beacons estimated by the proposed UWB-Foot-SLAM at the end of the experiment were colored in orange, green, yellow, and purple in Fig. 8.

Fig. 9 shows the position uncertainties of different states predicted by the EKF in the experiment. The horizontal position uncertainties in Fig. 9 were computed by summing the three times Standard Deviation (3σ) along the x- and the y-axis. The vertical uncertainties were the 3σ along the z-axis. Three observations could be made in Fig. 9. First, when the UWB beacons of the PEBBLE system were connected to the UWB module on the Lab-On-Shoe platform, the position uncertainties associated with the beacons were reduced. Second, At timestamps of 145 [s], the position uncertainty of the agent becomes larger than the position uncertainty of beacon #1 and #2. After this timestamp, the two beacons were considered localized and would start compensating for the position errors of the agents. Third, it could be seen that both the horizontal and vertical position uncertainties of the agent in the ZUPT-aided INS follow increasing trends while the uncertainties in the case of our proposed UWB-Foot-SLAM were reduced and bounded by the localized beacons.

The experimental results presented in Section IV-A and Section IV-B demonstrate that the proposed UWB-Foot-SLAM could simultaneously localize unknown beacons' positions with sufficiently high accuracy. Range measurements collected by the localized beacons could provide position compensation in the proposed approach, significantly improving long-term pedestrian navigation accuracy, as compared to a standalone ZUPT-aided INS.

C. Discussion

Several remarks could be made during navigation testing of the proposed UWB-Foot-SLAM:

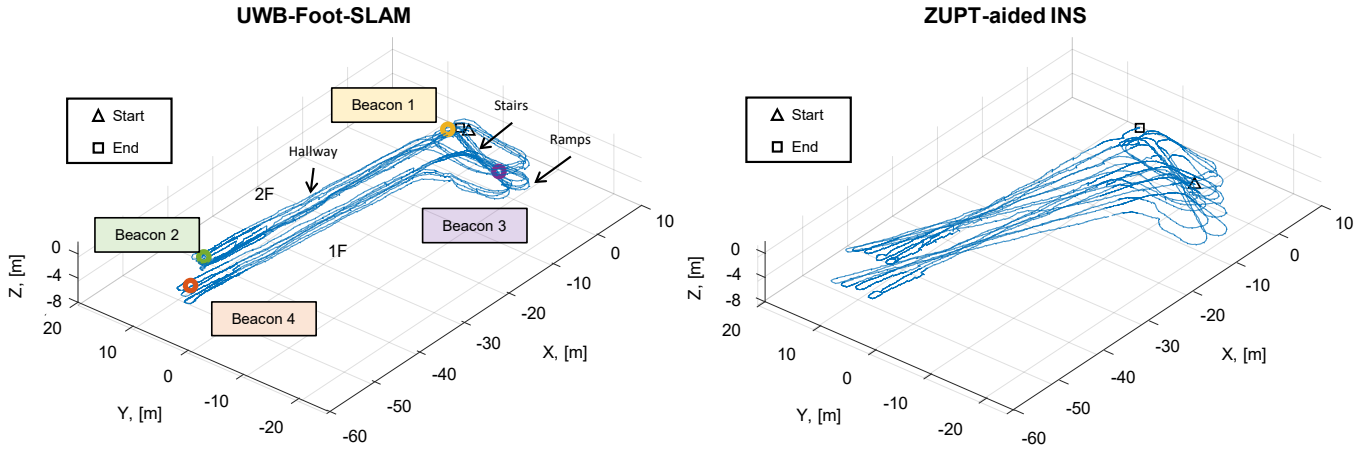

Fig. 8. Navigation solutions estimated by the proposed UWB-Foot-SLAM and a standalone ZUPT-aided INS in the experiment presented in Section IV-B.

- Initialization of UWB position states can affect accuracy of the beacon's estimated position. In the proposed approach, a beacon's position is initialized with an agent's current position. During the experiments presented in Section IV-A and Section IV-B, the agent deployed a beacon within reach, matching the design of our approach. However, the deployment could be done in a more flexible manner, such as by throwing beacons to distant locations. In such cases, the initialization mechanism discussed in this paper could lead to the estimated beacons' location being stuck in a statistical local minimum, degrading the navigation performance. One potential approach to address this issue is to use multiple initial guesses of a beacon's location, compute the likelihood of each guess, and select the one with the highest likelihood.
- The pattern of a pedestrian's navigation trajectory could affect the estimation accuracy of beacons' locations. This phenomenon is similar to the Position Dilution of Precision (PDOP) in other RF-signal-based positioning systems [31]. During our testings of the proposed UWB-Foot-SLAM algorithm, we observed that, when a pedestrian traveled only horizontally along a straight line, the estimated beacons' positions had significantly larger errors along the axes perpendicular to the direction of travel than those in parallel to the direction. The large errors could exceed the associated covariances, indicating existence of unmodeled errors in the estimation filter. It would be beneficial for future research to develop a multi-model approach to mitigate this issue.
- The ability to identify and compensate for NLoS UWB range measurements directly affects both the mapping and localization performance of our proposed UWB-Foot-SLAM. The experimental prototype discussed in Section III included foot-mounted UWB modules. This configuration was designed to avoid the need to estimate relative positions between a UWB and an IMU attached to a pedestrian. However, as compared to other mounting positions, such as head or shoulder, foot-mounted UWBs had more difficulties in receiving LoS measurements, as the modules were close to the ground and the direct signal path could be blocked by a pedestrian body part [29]. To improve the UWB range measurement accuracy, advanced LoS/NLoS detection and bias compensation approaches could be advantageous [32].
- The UWB-Foot-SLAM algorithm proposed in this paper was realized in a centralized framework, where all the states were updated in every iteration of the EKF, even if some of the beacons were not connected. The proposed UWB-Foot-SLAM could be extended to a de-centralized framework [33], which is computationally less expensive and would be more friendly to be implemented in real-time on a microcontroller. It would be beneficial to investigate the trade-offs between navigation performance and computational complexity of the centralized and de-centralized realizations.
- The performance of localization of pedestrians and mapping unknown beacons in our proposed UWB-Foot-SLAM depends on the performance of the built-in ZUPT-aided INS. Our proposed approach could be improved with an enhanced ZUPT-aided INS. The enhancement could be achieved on multiple different aspects of the system, including robust stance phase detection [34]–[36], self-contained sensor fusion solutions [13], [37]–[39], and IMU compensation [40], [41].

V. Conclusion

This paper proposed a UWB-Foot-SLAM algorithm that simultaneously localizes positions of a pedestrian and maps locations of unknown beacons. We developed an experimental prototype, including the Lab-On-Shoe platform and the PEBBLE system, and compared the performance of the proposed UWB-Foot-SLAM algorithm with a standalone ZUPT-aided INS in two different experiments. The first experiment involved evaluating the navigation solutions with a high-accuracy motion capture camera system. The ZUPT-aided INS

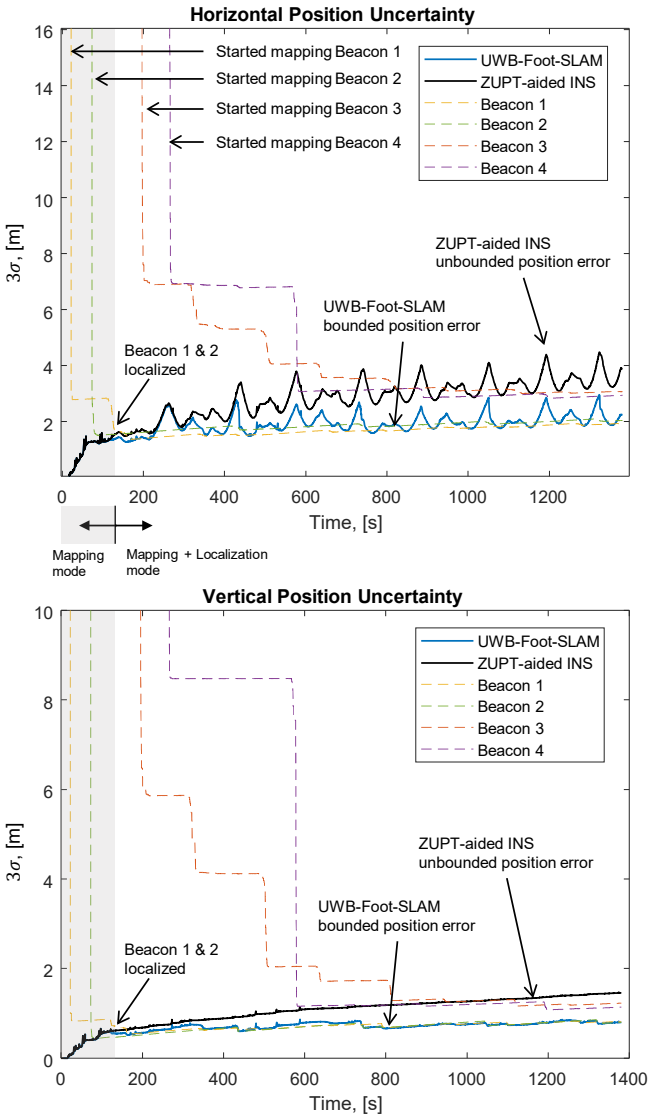

Fig. 9. Propagation profile of the covariances associated with agent's and beacon's positions. It could be seen that the agent's position uncertainties were bounded in the case of the UWB-Foot-SLAM while the uncertainties in the case of the ZUPT-aided INS followed an increasing trend.

had a position RMSE of 0.15 [m] and an LCE of 0.22 [m]. The proposed UWB-Foot-SLAM had a position RMSE of 0.15 [m] and an LCE of 0.27 [m]. Positions of the two UWB beacons estimated by the proposed UWB-Foot-SLAM had displacement errors of 0.28 [m] and 0.22 [m], respectively. In the second experiment, the ZUPT-aided INS had an LCE of 11 [m] along the horizontal direction and 4.5 [m] along the vertical direction. The proposed UWB-Foot-SLAM algorithm achieved an LCE of 1.49 [m] along the horizontal direction and 1 [m] along the vertical direction. The experimental result also showed that the EKF covariances associated with pedestrian's positions in the case of the proposed UWB-Foot-SLAM were bounded. The experimental results show that the proposed UWB-Foot-SLAM algorithm could significantly improve the long-term positioning accuracy of a pedestrian inertial navigation system using foot-mounted IMUs.

ACKNOWLEDGMENT

This work was performed using Federal funds under award 70NANB22H073 from the National Institute of Standards and Technology (NIST), U.S. Department of Commerce. The statements, findings, conclusions, and recommendations are those of the author(s) and do not necessarily reflect the views of NIST or the U.S. Department of Commerce.

Motion capture system data presented in Section IV-A was collected at the Public Safety Immersive Test Center (PSITC), a collaboration between The First Responder Network Authority and The National Institute of Standards and Technology's Public Safety Communications Research Division located in Boulder, CO.

REFERENCES

[1] R. Kleinman and C. Merkel, "Digital contact tracing for COVID-19," *Canadian Medical Association Journal*, vol. 192, no. 24, pp. E653–E656, 2020.

[2] B. Tejesh and S. Neeraja, "Warehouse inventory management system using IoT and open source framework," *Alexandria Engineering Journal*, vol. 57, no. 4, pp. 3817–3823, 2018.

[3] V. Renaudin, M. Ortiz, J. Perul, J. Torres-Sospedra, A. Jiménez, A. Pérez-Navarro, G. Mendoza-Silva, F. Seco, Y. Landau, R. Marbel, *et al.*, "Evaluating indoor positioning systems in a shopping mall: The lessons learned from the IPIN 2018 competition," *IEEE Access*, vol. 7, pp. 148594–148628, 2019.

[4] L. Sevrin, N. Noury, N. Abouchi, F. Jumel, B. Massot, and J. Saraydaryan, "Characterization of a multi-user indoor positioning system based on low cost depth vision (Kinect) for monitoring human activity in a smart home," in *International Conference of the IEEE Engineering in Medicine and Biology Society*, (Milan, Italy), Aug 25-29, 2015.

[5] A. Ferreira, D. Fernandes, A. Catarino, and J. Monteiro, "Localization and positioning systems for emergency responders: A survey," *IEEE Communications Surveys & Tutorials*, vol. 19, no. 4, pp. 2836–2870, 2017.

[6] T. Lemaire, C. Berger, I.-K. Jung, and S. Lacroix, "Vision-based SLAM: Stereo and monocular approaches," *International Journal of Computer Vision*, vol. 74, no. 3, pp. 343–364, 2007.

[7] G. Kumar, A. Patil, R. Patil, S. Park, and Y. Chai, "A LiDAR and IMU integrated indoor navigation system for UAVs and its application in real-time pipeline classification," *Sensors*, vol. 17, no. 6, pp. 1268–1291, 2017.

[8] Y. Zhuang, J. Yang, Y. Li, L. Qi, and N. El-Sheimy, "Smartphone-based indoor localization with bluetooth low energy beacons," *Sensors*, vol. 16, no. 5, pp. 596–615, 2016.

[9] Y. Shu, Y. Huang, J. Zhang, P. Coué, P. Cheng, J. Chen, and K. Shin, "Gradient-based fingerprinting for indoor localization and tracking," *IEEE Transactions on Industrial Electronics*, vol. 63, no. 4, pp. 2424–2433, 2015.

[10] K. Shamaei and Z. Kassas, "LTE receiver design and multipath analysis for navigation in urban environments," *NAVIGATION, Journal of the Institute of Navigation*, vol. 65, pp. 655–675, December 2018.

[11] A. Ruiz and F. Granja, "Comparing ubisense, bespoon, and decawave UWB location systems: Indoor performance analysis," *IEEE Transactions on Instrumentation and Measurement*, vol. 66, no. 8, pp. 2106–2117, 2017.

[12] D. Titterton and J. Weston, *Strapdown inertial navigation technology*, vol. 17. London, United Kingdom: IET, second ed., 2004.

[13] C.-S. Jao, A. A. Abdallah, C. Chen, M. Seo, S. S. Kia, Z. M. Kassas, and A. M. Shkel, "Sub-meter accurate pedestrian indoor navigation system with dual ZUPT-aided INS, machine learning-aided LTE, and UWB signals," in *International Technical Meeting of the Satellite Division of The Institute of Navigation (ION GNSS+ 2022)*, (Denver, CO, USA), Sep 19-23, 2022.

[14] Y. Wang, A. Chernyshoff, and A. M. Shkel, "Error analysis of ZUPT-aided pedestrian inertial navigation," in *International Conference on Indoor Positioning and Indoor Navigation*, (Nantes, France), Sep 24-27 2018.

[15] E. Foxlin, "Pedestrian tracking with shoe-mounted inertial sensors," *IEEE Computer Graphics and Applications*, vol. 25, no. 6, pp. 38–46, 2005.

[16] J.-O. Nilsson, A. K. Gupta, and P. Händel, "Foot-mounted inertial navigation made easy," in *International Conference on Indoor Positioning and Indoor Navigation*, (BEXCO, Busan, Korea), Oct 27-30, 2014.

[17] Y. Wang, C.-S. Jao, and A. Shkel, "Scenario-dependent ZUPT-aided pedestrian inertial navigation with sensor fusion," *Journal of Gyroscopy and Navigation*, vol. 12, no. 1, pp. 1–16, 2021.

[18] J.-O. Nilsson, I. Skog, and P. Händel, "A note on the limitations of ZUPTs and the implications on sensor error modeling," in *International Conference on Indoor Positioning and Indoor Navigation*, (Sydney, Australia), Nov 13-15, 2012.

[19] C.-S. Jao, A. Abdallah, C. Chen, M. Seo, S. S. Kia, Z. M. Kassas, and A. M. Shkel, "PINDOC: Pedestrian indoor navigation system integrating deterministic, opportunistic, and cooperative functionalities," *IEEE Sensors Journal*, vol. 22, pp. 14424–14435, July 2022.

[20] J. Zhu and S. S. Kia, "Cooperative localization under limited connectivity," *IEEE Transactions on Robotics*, vol. 35, no. 6, pp. 1523–1530, 2019.

[21] Y. Wang and X. Li, "An improved robust EKF algorithm based on sigma points for UWB and foot-mounted IMU fusion positioning," *Journal of Spatial Science*, vol. 66, no. 2, pp. 329–350, 2021.

[22] Y. Wang and X. Li, "The IMU/UWB fusion positioning algorithm based on a particle filter," *ISPRS International Journal of Geo-Information*, vol. 6, no. 8, p. 235, 2017.

[23] Y. Wang and X. Li, "Graph-optimization-based ZUPT/UWB fusion algorithm," *ISPRS International Journal of Geo-Information*, vol. 7, no. 1, p. 18, 2018.

[24] Y. Xu, X. Chen, J. Cheng, Q. Zhao, and Y. Wang, "Improving tightly-coupled model for indoor pedestrian navigation using foot-mounted IMU and UWB measurements," in *IEEE International Instrumentation and Measurement Technology Conference*, (Taipei, Taiwan), May 23-26 2016.

[25] Z. Zeng, S. Liu, W. Wang, and L. Wang, "Infrastructure-free indoor pedestrian tracking based on foot mounted UWB/IMU sensor fusion," in *2017 11th International Conference on Signal Processing and Communication Systems (ICSPCS)*, (Surfers Paradise, Australia), Dec 13-15 2017.

[26] R. Ali, R. Liu, A. Nayyar, B. Qureshi, and Z. Cao, "Tightly Coupling Fusion of UWB Ranging and IMU Pedestrian Dead Reckoning for Indoor Localization," *IEEE Access*, vol. 9, pp. 164206–164222, 2021.

[27] X. Li, Y. Wang, and D. Liu, "Research on extended Kalman filter and particle filter combinational algorithm in UWB and foot-mounted IMU fusion positioning," *Mobile Information Systems*, vol. 2018, 2018.

[28] I. Skog, P. Handel, J.-O. Nilsson, and J. Rantakokko, "Zero-velocity detection—an algorithm evaluation," *IEEE Transactions on Biomedical Engineering*, vol. 57, no. 11, pp. 2657–2666, 2010.

[29] C. Chen, C.-S. Jao, A. M. Shkel, and S. S. Kia, "UWB Sensor Placement for Foot-to-Foot Ranging in Dual-Foot-Mounted ZUPT-Aided INS," *IEEE Sensors Letters*, vol. 6, no. 2, pp. 1–4, 2022.

[30] S. Askari and C.-S. Jao and Y. Wang and A. M. Shkel, "A laboratory testbed for self-contained navigation," in *IEEE International Symposium on Inertial Sensors and Systems*, (Naples, FL, USA), Apr 1-5, 2019.

[31] R. B. Langley *et al.*, "Dilution of precision," *GPS world*, vol. 10, no. 5, pp. 52–59, 1999.

[32] J. Zhu and S. S. Kia, "Bias compensation for UWB ranging for pedestrian geolocation applications," *IEEE Sensors Letters*, vol. 3, no. 9, pp. 1–4, 2019.

[33] J. Zhu and S. S. Kia, "Decentralized cooperative localization with LoS and NLoS UWB inter-agent ranging," *IEEE Sensors Journal*, vol. 22, no. 6, pp. 5447–5456, 2021.

[34] E. Sangenis, C.-S. Jao, and A. M. Shkel, "SVM-based Motion Classification Using Foot-mounted IMU for ZUPT-aided INS," in *IEEE Sensors*, (Dalla, TX, USA), Oct 30-2, 2022.

[35] C.-S. Jao, Y. Wang, and A. M. Shkel, "A zero velocity detector for foot-mounted inertial navigation systems aided by downward-facing range sensor," in *2020 IEEE SENSORS*, (Virtual Conference), Oct 25-28, 2022.

[36] Y. Wang and A. M. Shkel, "Adaptive threshold for zero-velocity detector in ZUPT-aided pedestrian inertial navigation," *IEEE Sensors Letters*, vol. 3, no. 11, pp. 1–4, 2019.

[37] C.-S. Jao, Y. Wang, and A. M. Shkel, "Pedestrian inertial navigation system augmented by vision-based foot-to-foot relative position measurements," in *IEEE/ION Position, Location and Navigation Symposium (PLANS)*, (Virtual Conference), Apr 20-23, 2020.

[38] M. Laverne, M. George, D. Lord, A. Kelly, and T. Mukherjee, "Experimental validation of foot to foot range measurements in pedestrian tracking," in *the 24th International Technical Meeting of The Satellite Division of the Institute of Navigation (ION GNSS 2011)*, (Portland, OR, USA), Sep 20-23, 2011.

[39] A. A. Abdallah, C.-S. Jao, Z. M. Kassas, and A. M. Shkel, "A pedestrian indoor navigation system using deep-learning-aided cellular signals and ZUPT-aided foot-mounted IMUs," *IEEE Sensors Journal*, vol. 22, no. 6, pp. 5188–5198, 2021.

[40] C.-S. Jao, D. Wang, A. R. Parrish, and A. M. Shkel, "A neural network approach to mitigate thermal-induced errors in zupt-aided ins," in *IEEE International Symposium on Inertial Sensors and Systems (INERTIAL)*, (Avignon, France), May 8-11, 2022.

[41] C. Jao and A. Shkel, "A reconstruction filter for saturated accelerometer signals due to insufficient FSR in foot-mounted inertial navigation system," *IEEE Sensors Journal*, vol. 22, no. 1, pp. 695–706, 2021.